



Full Length Article

Core-shell structured ceramic nonwoven separators by atomic layer deposition for safe lithium-ion batteries



Xiu Shen^a, Chao Li^a, Chuan Shi^b, Chaochao Yang^c, Lei Deng^d, Wei Zhang^a, Longqing Peng^a, Jianhui Dai^c, Dezhi Wu^d, Peng Zhang^{c,*}, Jinbao Zhao^{a,c,*}

^a State Key Lab of Physical Chemistry of Solid Surfaces, Collaborative Innovation Center of Chemistry for Energy Materials, State-Province Joint Engineering Laboratory of Power Source Technology For New Energy Vehicle, College of Chemistry and Chemical Engineering, Xiamen University, Xiamen 361005, China

^b Industrial Research Institute of Nonwovens & Technical Textiles, Qingdao University, Qingdao 266071, China

^c School of Energy Research, College of Energy, Xiamen University, Xiamen 361102, China

^d School of Aerospace Engineering, Xiamen University, Xiamen 361005, China

ARTICLE INFO

Article history:

Received 7 October 2017

Revised 19 January 2018

Accepted 25 January 2018

Available online 31 January 2018

Keywords:

Core-shell structured separator

Atomic layer deposition

Lithium-ion batteries

Safety

ABSTRACT

Safety is one of the most factors for lithium-ion batteries (LIBs). In this work, a novel kind of ceramic separator with high safety insurance is proposed. We fabricated the core-shell nanofiber separators for LIBs by atomic layer deposition (ALD) of 30 nm Al₂O₃ on the electrospinning nonwoven fiber of polyvinylidene fluoride-hexafluoropropylene (PVDF-HFP). The separators show a pretty high heat resistance up to 200 °C without any shrinkage, an excellent fire-resistant property and a wide electrochemical window. Besides, with higher uptake and ionic conductivity, cells assembled with the novel separator shows better electrochemical performance. The ALD produced separators exhibit great potential in elaborate products like 3C communications and in energy field with harsh requirements for safety such as electric vehicles. The application of ALD on polymer fiber membranes brings a new strategy and opportunity for improving the safety of the advanced LIBs.

© 2018 Elsevier B.V. All rights reserved.

1. Introduction

With the continuously increasing demand of the energy consumption, lithium-ion batteries (LIBs) have been developed as one of the most attractive electrical power systems used in portable electronic devices and large scale energy storage systems like electric vehicles (EVs) [1–4] due to their high energy density, long cycle life, no memory effect, as well as low self-discharging [3]. Unfortunately, with tremendous applications of the LIBs used in our daily life, the safety problems have become more and more noticeable, especially after the explosion accident of the Galaxy Note 7 cellphone made in the Samsung Electronics.

The separator is a key safety related component of LIBs that can prevent electrodes from contact each other, and its dimensional stability, mechanical strength and melting point can also make a

big difference for the safety performance of batteries. Although commercial microporous polyolefin separators, such as polyethylene (PE), polypropylene (PP) and PP/PE/PP, have been widely used because of their excellent chemical stability and mechanical strength, they are still suffering from severe thermo-shrinkage at high temperature and poor wettability problems as well as high cost for the high quality products, which limit their further application in the electric vehicles (EVs) and large scale energy storage systems. In order to solve these questions, a lot of researches have been done to make sustained improvements for new and better separators.

Most reported modified separators can be divided into four types [3,5]: modified polyolefin separators [6–11], inorganic-organic composite separators [12–15], polymer electrolyte membrane [16–23] and nonwoven membrane [24–28]. Among those studies, the electrospinning of nonwoven separators is an effective, versatile controllable, multi-selective of substrate and economic way to make large scale microporous nonwoven separators [29]. Besides nonwoven separators have high porosity and great wettability. Various efforts have been made to fabricate special functional nonwoven separators. For example, very recently a core-shell flame-retardant nonwoven separator was prepared with triphenyl phosphate (TPP) as the core to suppress the combustion

* Corresponding authors at: State Key Lab of Physical Chemistry of Solid Surfaces, Collaborative Innovation Center of Chemistry for Energy Materials, State-Province Joint Engineering Laboratory of Power Source Technology For New Energy Vehicle, College of Chemistry and Chemical Engineering, Xiamen University, Xiamen 361005, China and School of Energy Research, College of Energy, Xiamen University, Xiamen 361102, China.

E-mail address: jbzhao@xmu.edu.cn (J. Zhao).

of the electrolyte at high temperature [25]. However, most commonly used electrospinning nonwoven polymers still have a thermal instability problem such as shrinkage at high temperature. And this problem can be easily solved by ceramic coating which has been reported to be successfully applied on industrial production. Our previous work reported a ceramic coating of Al_2O_3 mixed with carboxy methylated cellulose (CMC) and styrene butadiene rubber (SBR) water soluble binder, which showed great heat stability and wettability [30], and a polydopamine (PDA) coating on ceramic separator, which was thermally and mechanically stable even at 230 °C [31]. Nevertheless, the present ceramic coating on nonwoven separators is efficient to improve wettability and the heat tolerance of the separator, and thus enhance the safety of batteries, but the several micron thickness coating layer will increase the thickness and mass of the separator obviously and then decrease the energy density of the whole battery to some degree [32]. Therefore, decrease of the thickness and mass of the ceramic coating layer is one of the urgent demands for nonwoven separators for high density and high safety batteries.

Atomic layer deposition (ALD) is a technique to induce an ultrathin and conformal layer with precise thickness control and uniformity by a self-limiting reaction mechanism [33,34]. It has been widely used to make a modifying or protective coating layer on original materials and devices for the semiconductor industry [33,35]. Recent years, the ALD technology has been used to design high performance components of cathodes [36,37], anodes [36,38,39] and polyolefin separators [40–42] for lithium ion batteries. The resulting nanostructures can attribute to form better LIBs with high energy density, high safety, low cost and long service life because of ALD's low growth temperature, atomic scale deposition and outstanding uniformity and conformality [43]. Except for acting as a versatile and tunable technique to synthesis LIBs components, ALD is also applied to precisely grow ultrathin films on electrodes and electrolytes [44]. Previous study applied the classic ALD in polyolefin separators has been proven to be effective to functionalize the membranes with good wettability and thermal stability and, at the same time, without obvious increase of thickness and mass. The plasma enhancement before the ALD process is an alternative route to generate highly reactive radicals and ions and reduce the growth temperature [34,45].

In this work, we have designed and fabricated a novel core-shell composite nonwoven separator, polyvinylidene fluoride-hexafluoropropylene (PVDF-HFP) $\text{@Al}_2\text{O}_3$, by the ALD of Al_2O_3 on the electrospinning nonwoven separator. The plasma treatment before the traditional ALD process can provide active oxygen-contained sites to bond with the ALD precursor source for better deposition. The battery separators after ALD treatment show drastically improved safety performance, among which excellent thermal tolerance and great fire resistance are emphasized here. Besides, other physical characterization and electrochemical test are examined also.

2. Experimental details

2.1. Fabrication of PVDF-HFP $\text{@Al}_2\text{O}_3$ separator

The process is mainly comprised of two steps: the preparation of the electrospinning fiber mat of PVDF-HFP, and the encapsulation of the ultrathin Al_2O_3 layer on the polymer fiber. To make nonwoven mat of electrospinning PVDF-HFP fiber, the 16 wt% spinning solution was made as the following process: well dissolved PVDF-HFP (Aldrich, $M = 45,500\text{--}110,000$) in the hybrid solvent of *N*-methyl pyrrolidone (NMP)/acetone with volume ratio of 1:1 by magnetic stirring for 8 h. The electrospinning process was achieved through a self-assembled electrospinning setup with a high voltage

power supply, an inject pump and a copper plate as collector. The feed rate of the PVDF-HFP solution was 300 $\mu\text{l/h}$ under 10 kV, with a 15 cm distance between the nozzle tip and the copper collector. As-prepared nonwoven fiber matrix was first dried in an air-circulating oven at 60 °C for 4 h, and then stored in vacuum oven at 60 °C for 12 h.

The produced fiber mat was treated by oxygen reaction ion etching (RIE) first at 50 W for 20 s for the plasma enhancement. It is emphasized here that oxygen-derived free radicals can be formed on the polymer surface. The membrane was quickly transferred into the chamber of the ALD system (Picosun Oy, R-200 Advanced) within 20 min. Using TMA ($\text{Al}(\text{CH}_3)_3$, 95%) as the alumina precursor and the deionized water as oxygen source, the reaction proceeded at 70 °C by sequential exposures of TMA and H_2O . A certain cycle is composed of TMA pulse for 0.1 s, N_2 purge for 15 s, H_2O pulse for 0.1 s, and N_2 purge for 30 s. The flow rate of N_2 was 50 sccm (standard cm^3/min). After 150 reaction cycles of $\text{Al}(\text{CH}_3)_3/\text{H}_2\text{O}$ for each side, the final separator was obtained.

2.2. Assembling of coin cells

Coin cells (CR 2016) with LiMn_2O_4 (LMO) cathode and lithium tablet anode were assembled in a high-purity argon-filled glove box (Braun) for electrical performance test. 90 wt% LiMn_2O_4 (Qingdao Xinzheng Material Co., Ltd, China), 5 wt% acetylene black (AB), and 5 wt% PVDF were mixed in NMP to prepare the cathode of the cell. The electrolyte used was consisted with ethylene carbonate (EC) and dimethyl carbonate (DMC) (1:1, weight ratio, Zhangjiagang Guotaihuarong New Chemical Materials Co., Ltd). PP separators and nonwoven separators of PVDF-HFP and PVDF-HFP $\text{@Al}_2\text{O}_3$ were assembled respectively for the LMO batteries.

2.3. Characterization of the separators

A field emission scanning electron microscope (FESEM, Hitachi S-4800) operated at 15 kV was used to view the morphology of the separator. The diameter distribution and average value of the separator fibers were statistically analyzed via the Image Pro Plus software. And the energy dispersive X-ray spectroscopy (EDX, Hitachi S4800) was applied to make the elementary analysis. The field emission transmission electron microscopy (TEM, JEM-1400) was also applied to obtain the structure of as-prepared membrane. Thermogravimetric (TG) was performed from 35 °C to 800 °C at the heating rate of 5 °C/min in air on a Model STA 449 instrument (NETZSCH Machinery and Instruments Co., Ltd) to further analyze the thermal behavior and composition of the separator. Fourier transform infrared spectroscopy (FTIR) study of separators was also carried out on a Nicolet IS5 spectrometer (Thermo Fisher Scientific Inc.) in the range of 400–4000 cm^{-1} . X-ray photoelectron spectroscopy (XPS) was performed to further determine the surface element compositions of the separators.

Thermal stability tests of commercial PP, bare PVDF-HFP and the ALD separators under different temperatures were performed by storing them in an air-circulating drying oven for 30 min. And the separators were sandwiched between two glass plates when tested. The fire resistance of the PVDF-HFP separators before and after the ALD process was studied in order to further demonstrate the safety property of the separators. The OCV curves at 160 °C was recorded of the fully charged LiFePO_4 (LFP)/Graphite (G) full cells (LFP/G/PVDF = 8:1:1) with different separators. Contact angle changes were also tested by using a contact angle goniometer (Powereach JC2000C1, Shanghai Zhongchen Digital Technique Equipment Co., Ltd) with the same electrolyte for the 2016 coin cells. Electrolyte uptake (EU) are measured and calculated by the following equation:

$$EU(\%) = (m - m_0)/m_0 \times 100\%$$

where m_0 and m are the mass of the separators before and after soaked in electrolyte, respectively. The ionic conductivity (σ) was investigated and calculated by electrochemical impedance spectroscopy (EIS) using Autolab (Sino-Metrohm Technology Ltd) with a frequency range of 0.1–10⁵ Hz. The ionic conductivity related to porosity, thickness and tortuosity is calculated by the following equation:

$$\sigma = L/(R_b \times S)$$

where L is the thickness of the separator, R_b is the bulk resistance of the separator obtained by the EIS test, S is the area of the copper electrode. The linear sweep voltammograms (LSV) of Li/separator/stainless steel (SS) cell at a scan rate of 5 mV/s was measured in order to test the stability of the ALD separator. To investigate the electrochemical performance, the assembled CR2016 was load on a battery testing system (LAND-V34, Wuhan LAND Electronics Co., Ltd.). Battery cycle performances at a current rate of 1C in the voltage range of 3–4.2 V was measured for 100 cycles. And rate capabilities with the charge/discharge current sequence of 0.5 C, 1 C, 2 C, 5 C, 10 C and 0.5 C were measured to investigate the rate performance of the separators.

3. Results and discussion

The morphology of pristine commercial Celgard PP (25 μm), bare PVDF-HFP (40 \pm 2 μm) and the prepared separator PVDF-HFP@Al₂O₃ (42 \pm 2 μm) are shown in Fig. 1a–c, respectively. The bare PVDF-HFP and the ALD separator have the average fiber diameter of around 450 nm and 500 nm, respectively. TEM image of PVDF-HFP@Al₂O₃ separator (Fig. 1d) shows a core-shell structure, and the thickness of the ALD-Al₂O₃ shell is around 30 nm.

To ensure that the deposition of Al₂O₃ took place over all the nonwoven separator and deep into its inner area, the energy dispersive spectrometer (EDS) element mapping and EDS spectra were applied for the separator's cross section. As shown in Fig. 2, the distribution of the Al and O is throughout the whole composite nonwoven membrane, indicating a uniform deposition. And the EDS result displays that the O/Al atom ratio (1.506) is close to the theoretical value (1.5), conforming the formation of Al₂O₃.

The effects of the O₂ plasma and ALD process were further characterized by FTIR and XPS. As shown in Fig. 3a, compared with the bare PVDF-HFP, the PVDF-HFP@Al₂O₃ shows a broad absorption peak at around 600 cm⁻¹ which is ascribed to the Al–O bond of the Al₂O₃ bulk vibrational mode. And an absorption band around 3400 cm⁻¹ is also clearly observed due to the terminated -OH on the Al₂O₃ surface. The separator after O₂ plasma treatment (PVDF-HFP-Plasma) shows two small peaks at 1759 cm⁻¹ and 1852 cm⁻¹. The 1759 cm⁻¹ one is corresponding to the C=O bond stretching vibration of carbonyl under the inductive effect of α -F; the other at higher frequency of 1852 cm⁻¹ should be attributed to the vibration coupling of carbonyl, indicating the generation of oxygen active site [46,47]. And this can be verified by the XPS results. As shown in Fig. 3b, no evident signal of oxygen element is detected on the surface of the bare PVDF-HFP separator, while after plasma at 50 W for 20 s, the O1s characteristic peak located at 530.8 eV is found obviously, which verifies the success of O₂ plasma, agreeing well with the result of FTIR. The effect of oxygen plasma is considered to form active sites for better ALD of Al₂O₃ in the next step. In this case, the schematic diagram of the principle (Scheme 1a) and final product structure (Scheme 1b) of the ALD was given in Scheme 1. And after ALD process, the XPS peak assigned to F disappears, indicating the successful coating of the Al₂O₃ of ALD on the polymer fiber surface.

The increased mass of the ALD Al₂O₃ separator was measured by TG. As shown in Fig. 3c, the final residue is down to 0 for the

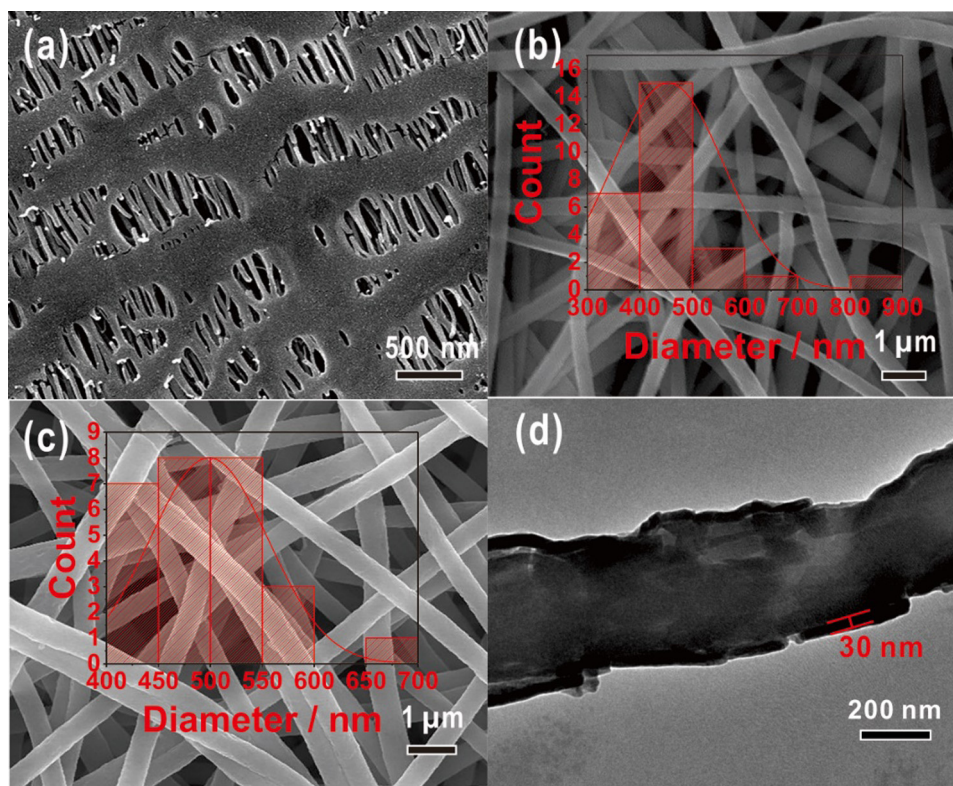


Fig. 1. SEM image of (a) PP, (b) PVDF-HFP and (c) PVDF-HFP@Al₂O₃, and (d) TEM micrograph of the PVDF-HFP@Al₂O₃ fibers.

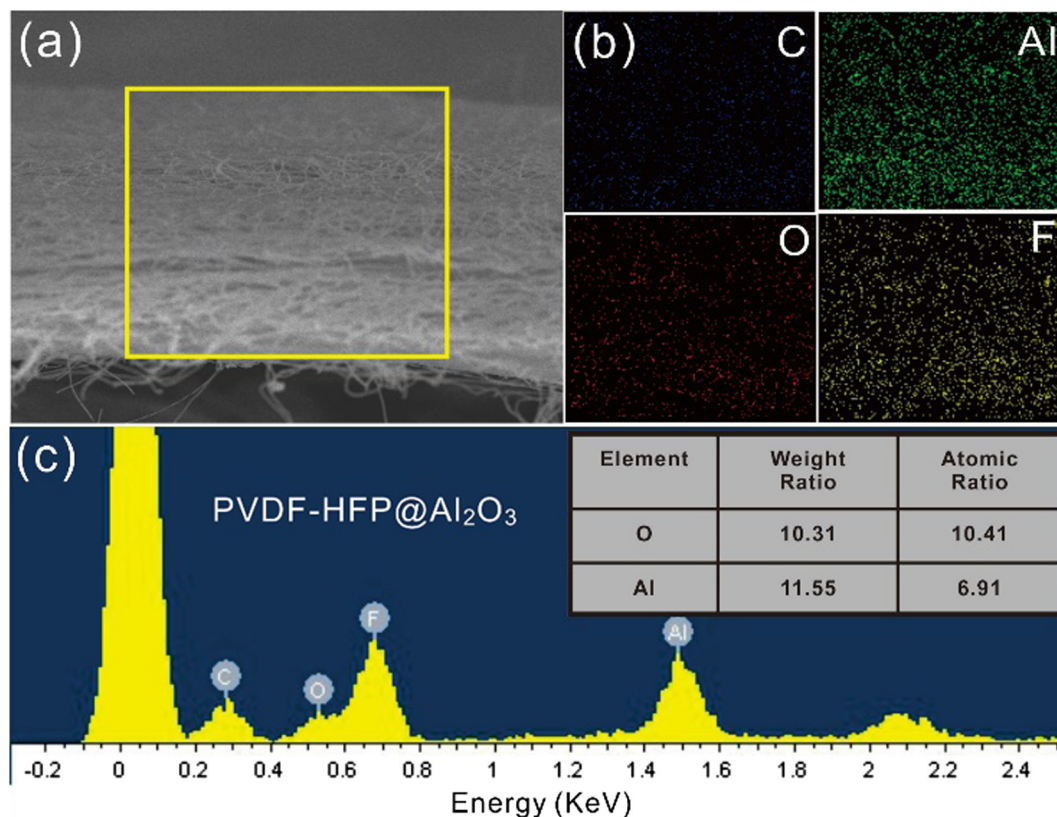


Fig. 2. EDS element mapping (a, b) and EDS spectra (c) of the cross section of PVDF-HFP@Al₂O₃ separator.

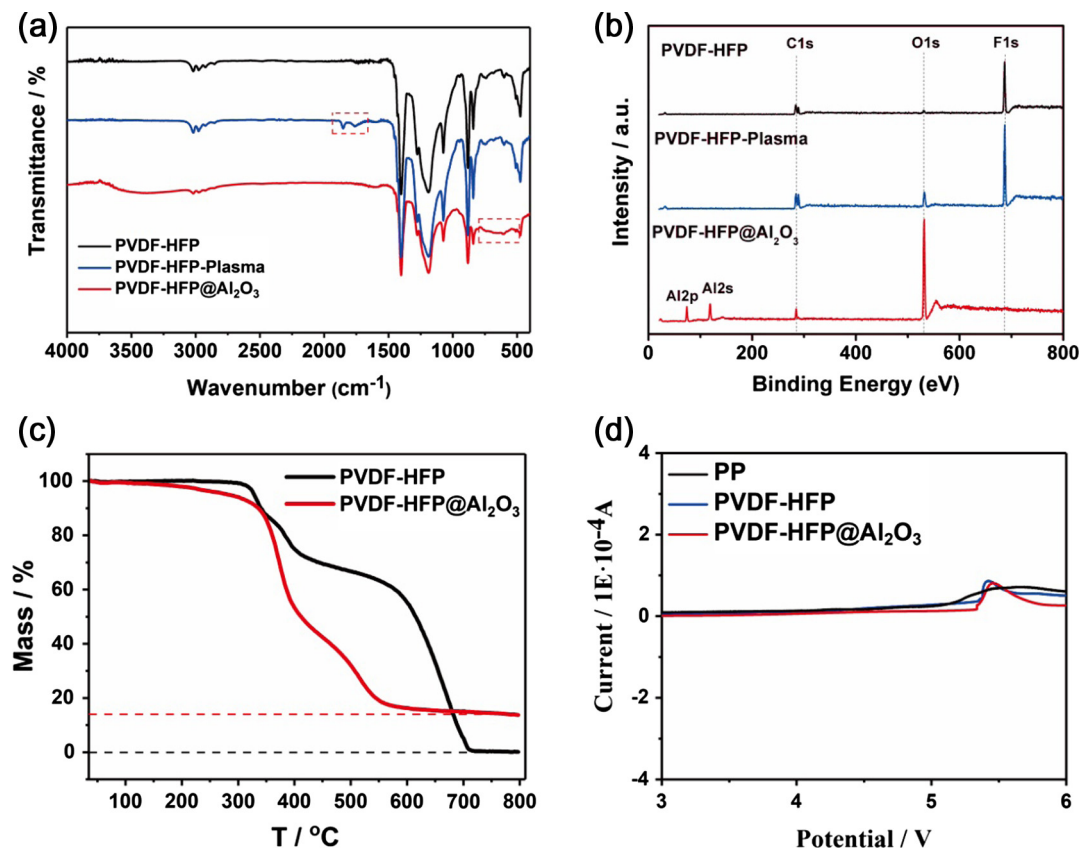
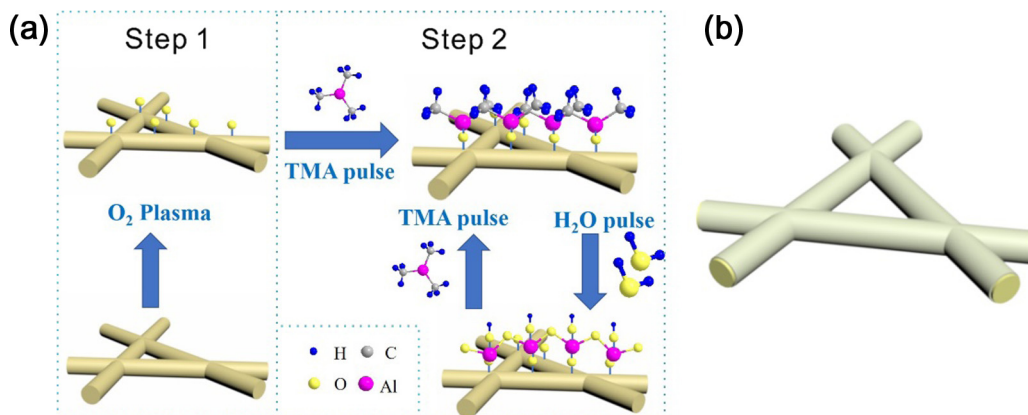


Fig. 3. FTIR (a) and XPS (b) of the PVDF-HFP, PVDF-HFP-Plasma and PVDF-HFP@Al₂O₃, (c) TG curves from 35 to 800 °C in air flow for the bare PVDF-HFP and the PVDF-HFP@Al₂O₃ separator, (d) The LSV curves of the PP, PVDF-HFP and PVDF-HFP@Al₂O₃ at the scan rate of 5 mV/s.



Scheme 1. Schematic diagram for (a) the principle and the fabrication steps and (b) the final core shell structure of ALD Al_2O_3 nonwoven separators.

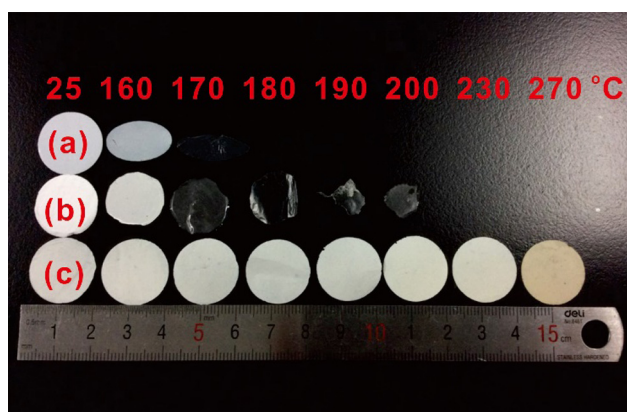


Fig. 4. Photos of (a) commercial PP, (b) bare PVDF-HFP, and (c) PVDF-HFP@ Al_2O_3 and their macroscopic changes after heat treatment at different temperatures.

bare PVDF-HFP, and the ALD Al_2O_3 coating separator has 13% mass left, revealing a thin thickness of the shell coating layer on polymer fibers. The electrochemical stability windows of the PP, PVDF-HFP and PVDF-HFP@ Al_2O_3 separators assembled respectively as the Li/

separator/SS cells are shown by the LSV in Fig. 3d. The LSV result is mainly related to the oxidation potential of the electrolyte. The PVDF-HFP@ Al_2O_3 separator shows no obvious decomposition below 5 V, suggesting great electrochemical stability. Compared with the electrochemical window of pristine nonwoven separator and PP, there is few side effect for the introduced ALD Al_2O_3 layer.

The thermal stability of separators was determined via the thermo-shrinkage test by storing separators sandwiched between two glasses in a drying oven at a series temperatures from 160 °C to 270 °C each for 30 min. Fig. 4 shows that the PVDF-HFP@ Al_2O_3 separator does not shrink even at 270 °C but turns yellow, and the PP and PVDF-HFP with similar melting point around 165 °C both shrink at 160 °C and turn transparent after 170 °C. The results demonstrate an excellent thermal stability advantage of the ALD separator over both bare commercial PP and PVDF-HFP. The introduction of the ultra-thin high heat tolerance ALD Al_2O_3 layer outside the polymer significantly enhanced the thermal stability of the separators, which greatly increased the safety of the battery.

In order to make clear the morphology changes of the separators after heat treatment, the SEM images of three separators corresponding to Fig. 4 are shown in Fig. 5. The commercial PP has microporous pores which are entirely shutdown at 170 °C

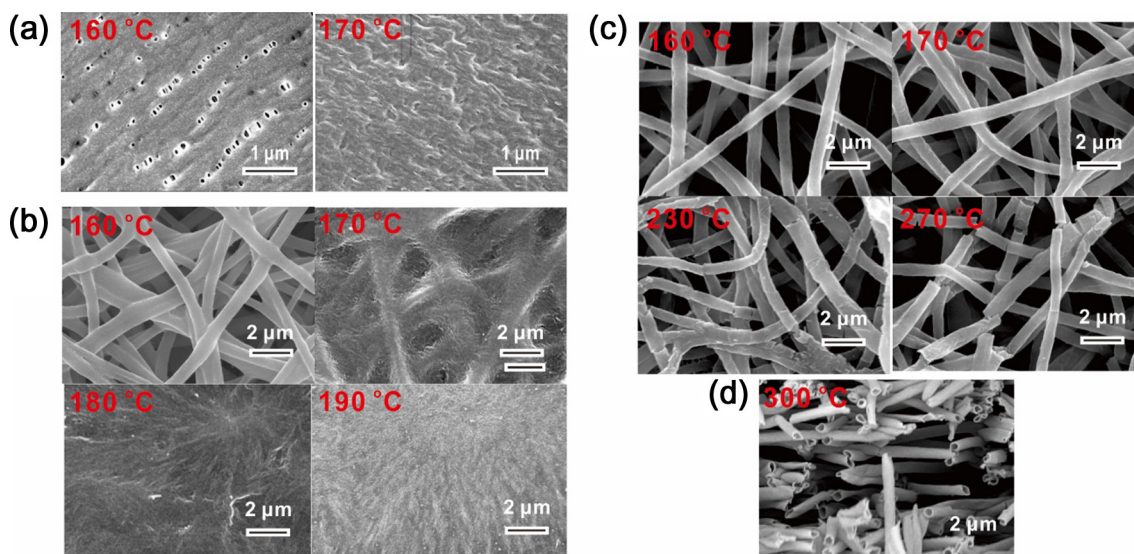


Fig. 5. SEM images of (a) commercial PP, (b) PVDF-HFP and (c) PVDF-HFP@ Al_2O_3 separator and their morphologies after heat treatment under different temperatures, (d) the cross section of the PVDF-HFP@ Al_2O_3 under 300 °C without sandwiched between two glasses.

(Fig. 5a), and the PVDF-HFP has turned into ribbon type at 160 °C due to its melting and then gradually crystallized when after 170 °C (Fig. 5b), but the PVDF-HFP@Al₂O₃ has shown few obvious change until fractures appeared at 270 °C indicating a trend of

pulverizing (Fig. 5c). Such excellent thermal stability after the ALD process is because of the coating of the ultrathin ceramic layer onto every single polymer fiber, forming a core-shell structure which can be seen from the TEM image (Fig. 1d) as well as the cross

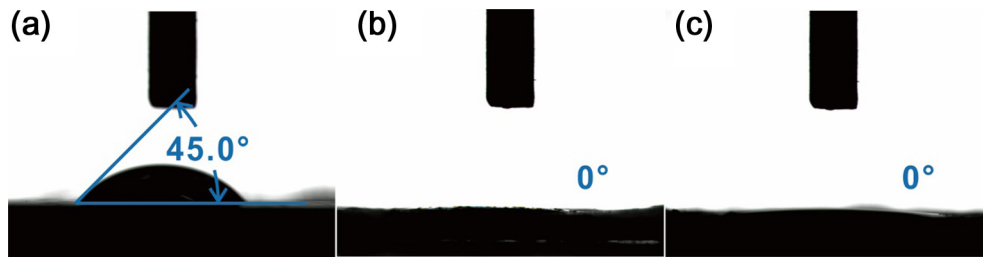


Fig. 6. The equilibrium contact angle of (a) PP, and (b) PVDF-HFP, and (c) PVDF-HFP@Al₂O₃.

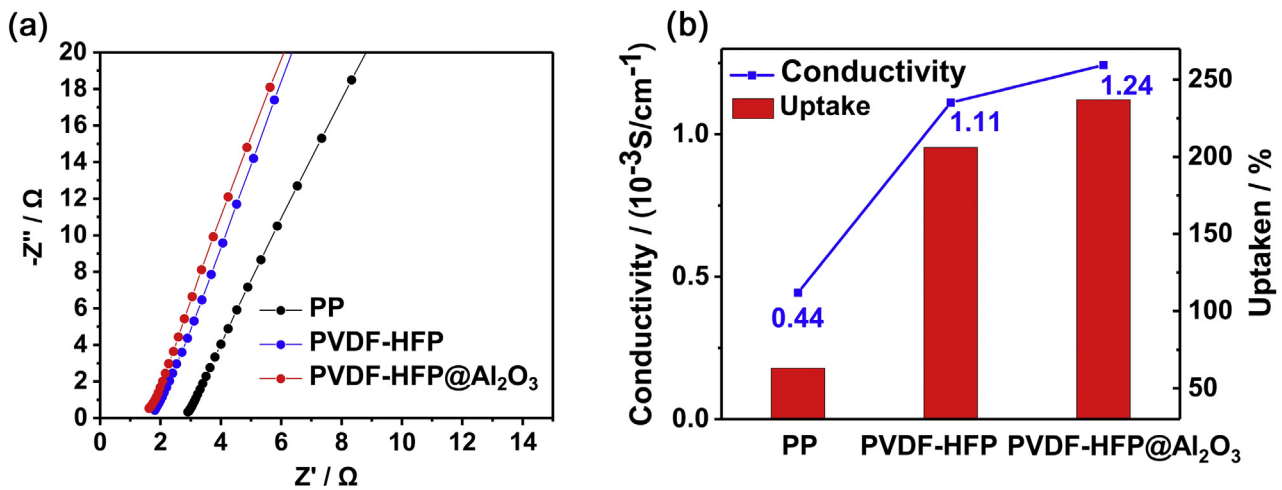


Fig. 7. (a) Nyquist plot of AC impedance measurements (ss/separator/ss) and (b) ionic conductivity and electrolyte uptake diagram of the PP, PVDF-HFP and PVDF-HFP@Al₂O₃ membrane.

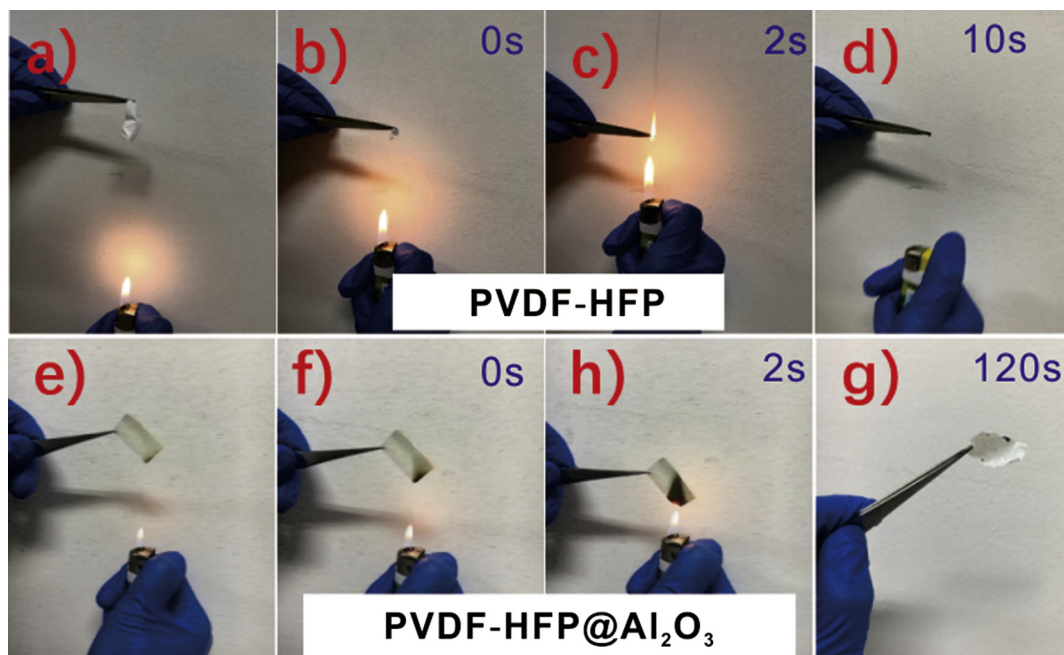


Fig. 8. Optical photographs of the flame retardant behavior of the PVDF-HFP and PVDF-HFP@Al₂O₃ separators taken with the flame approaching (a, e) and after ignited for different time (b–d, f, h, g).

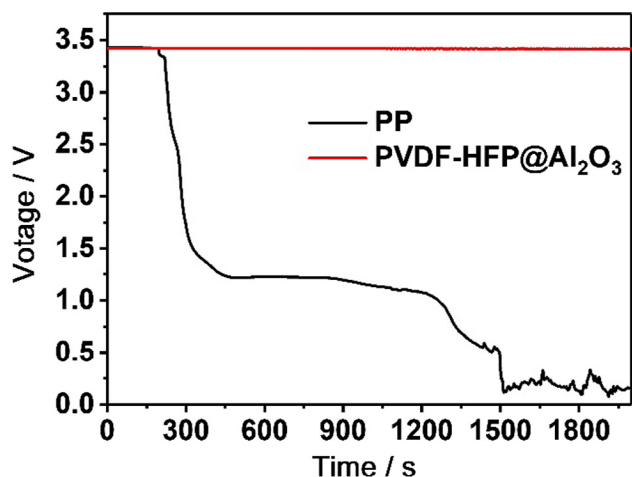


Fig. 9. The OCV curves at 160 °C of LFP/G full cells with different separators.

section SEM image (Fig. 5d). The cross section shows lots of nanotubes of the PVDF-HFP@Al₂O₃ after treatment at 300 °C for 30 min without glasses sandwiching. The forming of nanotubes is due to the melting of the polymer fiber core and oriented shrinkage onto the inter wall of the thermal stable Al₂O₃ coating layer. Without this coating layer, the polymer fiber will melt and cannot maintain the 1D structure or form nanotubes. This reveals that the Al₂O₃ is uniformly coated on the surface of the fibers forming core-shell structure. In addition, combining with the shrinkage test, 200 °C is a reasonable threshold operating temperature for the PVDF-HFP@Al₂O₃ separator.

In order to characterize the wettability of the separators to electrolyte, the contact angles of the PP, PVDF-HFP and PVDF-HFP@Al₂O₃ were measured with the electrolyte. As shown in Fig. 6, the equilibrium contact angle of the PVDF-HFP@Al₂O₃ (0°) and PVDF-HFP (0°) are smaller than that of PP separator (45.0°), indicating of an excellent wettability of the nonwoven separator than polyolefin separator. This is due to the high porosity of

nonwoven separators and the great affinity of nonwoven separators to the electrolyte.

Nyquist plots (Fig. 7a) of EIS tests show bulk resistance value of 2.8, 1.8 and 1.6 Ω of PP, PVDF-HFP and PVDF-HFP@Al₂O₃ separator and the corresponding conductivity of are 0.44, 1.11 and 1.24 mS cm⁻¹, respectively, increasing slightly after the ALD process. These results are consistent with increase of the electrolyte uptake due to the great affinity of Al₂O₃ to the electrolyte (Fig. 7b).

The fire resistance is a key aspect for the safety performance of the separator. It would benefit for the safety of the batteries if a complete coating of noncombustible cloth onto the separator could be successfully formed. As shown in Fig. 8, early in combustion process, the bare PVDF-HFP shrinks immediately as the flame approaches (Fig. 8a, b), but the PVDF-HFP@Al₂O₃ shows no obvious shrinkage and turns dark due to the carbon deposit (Fig. 8e, f). After ignited for 2 s, a flame tongue forms (Fig. 8c) but it extinguishes immediately for the PVDF-HFP separator due to the self-quenching function of F-containing polymers, while the PVDF-HFP@Al₂O₃ almost remains as a self-supporting membrane without flame (Fig. 8g). Upon completion of the combustion after 10 s, the PVDF-HFP membrane has turned into carbon compounds and dropt down, but for the ALD sample, after 120 s an ultrathin feeble white sheet composed of the ALD Al₂O₃ is left. And this test demonstrates that the ultrathin ceramic coating of Al₂O₃ by ALD process can effectively suppress the combustion of the separator and offer a high insurance for the battery safety. This is mainly due to that alumina is one of the best refractory materials.

In order to analysis the safety performance of the separator in real battery systems, the open circuit voltage (OCV) tests at 160 °C was carried out with full cells with LiFePO₄ as cathode, graphite as anode and LiClO₄/EC/PC as electrolyte. As shown in Fig. 9, the voltage of the cell with PP separator dropped sharply after 300 s and approached to 0 V after about 1500 s. However, potential of PVDF-HFP@Al₂O₃ separator maintain stable at the initial level, which shows a pretty high thermal stability of the novel core-shell structured separator in real battery systems.

In order to assess the electrochemical performance of batteries with as-prepared separator, the cycling and rate performance were

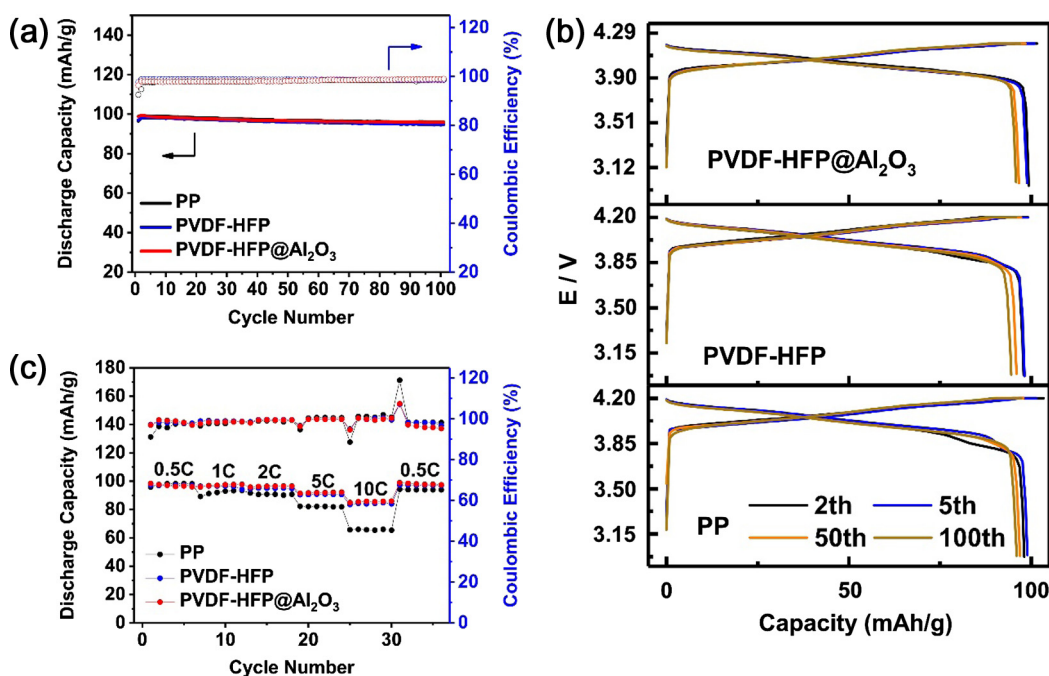


Fig. 10. Cycle performance (a) and rate property (b) of batteries with PP, PVDF-HFP and PVDF-HFP@Al₂O₃ separators.

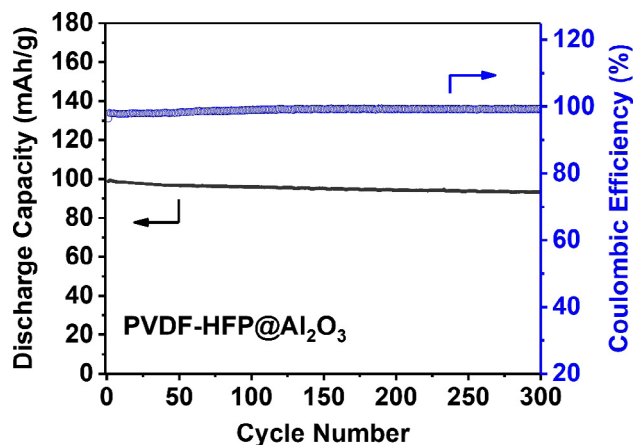


Fig. 11. Long cycle performance of batteries with PVDF-HFP@Al₂O₃ separators.

tested and shown in Fig. 10. The Li/PVDF-HFP@Al₂O₃/LMO coin cells were assembled and used for testing within the voltage range of 3–4.2 V (vs Li⁺/Li) at 1C, and the cells with commercial PP and bare PVDF-HFP were also assembled as comparison. As shown in Fig. 10a, cells with PP, PVDF-HFP, PVDF-HFP@Al₂O₃ show first discharge capacity of 96.40, 96.99, 98.88 mAh/g and coulombic efficiency of 92.56%, 97.73% and 96.41%, respectively. The ALD separator shows higher discharge capacity and higher coulombic efficiency than commercial PP due to the higher porosity and higher ionic conductivity. And these cells show identical capacity maintained ratio over 96.5% after 100 cycles, and all of them show the coulombic efficiency of near 100%. More detail charge-discharge curves of different cycles have been taken out and given in Fig. 10b. Cycling test indicates that the batteries with PVDF-HFP@Al₂O₃ has good cycling stability besides its great thermal stability and flame retardant property.

Rate performance of the LiMn₂O₄/Li coin cells with the three kinds of separators was also examined (Fig. 10c) to further investigate the electrochemical performance. All of their discharge capacities decrease gradually with the current rate increasing, and could go back to the initial level as the rate comes back to 0.5C. The discharge C-rate capacities of PVDF-HFP@Al₂O₃ separator cell is higher than that of PVDF-HFP or PP cell. And the difference among three separators became larger at higher discharge current rate, which is in conformance with their electrolyte uptake and ionic conductivity. At high rate of 10 C, the capacity of PVDF-HFP@Al₂O₃, PVDF-HFP and PP could be maintained at 68.51%, 85.90%, and 86.3% of the initial capacity at 0.5 C, indicating a great rate performance of the PVDF-HFP@Al₂O₃ cell. The enhanced rate performance of the core-shell structured separator is due to the high electrolyte uptake and high ion conductivity. In order to make sure the long cycle stability, 300 cycles was applied on the cell with PVDF-HFP@Al₂O₃ (Fig. 11), the result shows a capacity maintained ratio of 94.52% and a high coulombic efficiency over 99% during cycling.

4. Conclusion

A novel ceramic composite nonwoven separator with the core-shell structure for lithium-ion batteries has been fabricated. The new separator is prepared by electrospinning of polymer and then depositing of Al₂O₃ onto the fiber mat via ALD technique. As-fabricated separator has remarkable thermal stability and fire resistance property, which substantially improve the safety insurance for lithium-ion batteries. Besides, the separator shows great

electrochemical stability. At the same time, stable cycling performance and great rate performance are shown which are consistent with the high electrolyte uptake ratio and the high ionic conductivity. A small disadvantage of the PVDF-HFP@Al₂O₃ separator is the cost of the ALD process which depends on the development of the ALD technique.

Acknowledgement

The authors gratefully acknowledge financial support from the National Natural Science Foundation of China [Grant Numbers 21503180, 21273185, 21621091], the Fundamental Research Funds for the Central Universities [Grant Number 20720170037] and the National Key Research and Development Program of China [Grant Number 2017YFB0102000]. This work has also been supported by National Found for Fostering Talents of Basic Science [Grant Number J1310024]. The authors also wish to express their thanks to Dr. Daiwei Liao of Xiamen University for his valuable suggestions.

References

- [1] J.B. Goodenough, Y. Kim, Challenges for rechargeable Li batteries, *Chem. Mater.* 22 (2010) 587–603.
- [2] Jang Wook Choi, Doron Aurbach, Promise and reality of post-lithium-ion batteries with high energy densities, *Nature Rev. Mater.* 1 (2016) 16013.
- [3] H. Lee, M. Yanilmaz, O. Toprakci, K. Fu, X. Zhang, A review of recent developments in membrane separators for rechargeable lithium-ion batteries, *Energy Environ. Sci.* 7 (2014) 3857–3886.
- [4] V. Etacheri, R. Marom, R. Elazari, G. Salitra, D. Aurbach, Challenges in the development of advanced Li-ion batteries: a review, *Energy Environ. Sci.* 4 (2011) 3243.
- [5] S.S. Zhang, A review on the separators of liquid electrolyte Li-ion batteries, *J. Power Sources* 164 (2007) 351–364.
- [6] P.J. Zuo, J.F. Hua, M.X. He, H. Zhang, Z.Y. Qian, Y.L. Ma, C.Y. Du, X.Q. Cheng, Y.Z. Gao, G.P. Yin, Facilitating the redox reaction of polysulfides by an electrocatalytic layer-modified separator for lithium-sulfur batteries, *J. Mater. Chem. A* 5 (2017) 10936–10945.
- [7] K. Liu, D. Zhuo, H.W. Lee, W. Liu, D.C. Lin, Y.Y. Lu, Y. Cui, Extending the life of lithium-based rechargeable batteries by reaction of lithium dendrites with a novel silica nanoparticle sandwiched separator, *Adv. Mater.* 29 (2017).
- [8] K. Liu, P. Bai, M.Z. Bazant, C.-A. Wang, J. Li, A soft non-porous separator and its effectiveness in stabilizing Li metal anodes cycling at 10 mA cm⁻² observed in situ in a capillary cell, *J. Mater. Chem. A* 5 (2017) 4300–4307.
- [9] C. Li, P. Zhang, J. Dai, X. Shen, Y. Peng, Y. Zhang, J. Zhao, Rational method for improving the performance of lithium-sulfur batteries: coating the separator with lithium fluoride, *ChemElectroChem* (2017).
- [10] Z.A. Ghazi, X. He, A.M. Khattak, N.A. Khan, B. Liang, A. Iqbal, J.X. Wang, H.S. Sin, L.S. Li, Z.Y. Tang, MoS₂/Celgard separator as efficient polysulfide barrier for long-life lithium-sulfur batteries, *Adv. Mater.* 29 (2017) 6.
- [11] J. Fang, A. Kelarakis, Y.-W. Lin, C.-Y. Kang, M.-H. Yang, C.-L. Cheng, Y. Wang, E.P. Giannelis, L.-D. Tsai, Nanoparticle-coated separators for lithium-ion batteries with advanced electrochemical performance, *Phys. Chem. Chem. Phys.* 13 (2011) 14457–14461.
- [12] M. Wang, X. Chen, H. Wang, H. Wu, X. Jin, C. Huang, Improved performances of lithium-ion batteries with a separator based on inorganic fibers, *J. Mater. Chem. A* 5 (2017) 311–318.
- [13] S. Kim, T. Han, J. Jeong, H. Lee, M.H. Ryou, Y.M. Lee, A flame-retardant composite polymer electrolyte for lithium-ion polymer batteries, *Electrochim. Acta* 241 (2017) 553–559.
- [14] N. Chen, Y. Dai, Y. Xing, L. Wang, C. Guo, R. Chen, S. Guo, F. Wu, Biomimetic ant-nest ionogel electrolyte boosts the performance of dendrite-free lithium batteries, *Energy Environ. Sci.* (2017).
- [15] X. He, Q. Shi, X. Zhou, C. Wan, C. Jiang, In situ composite of nano SiO₂-P(VDF-HFP) porous polymer electrolytes for Li-ion batteries, *Electrochim. Acta* 51 (2005) 1069–1075.
- [16] H. Zhang, C. Li, M. Piszcz, E. Coya, T. Rojo, L.M. Rodriguez-Martinez, M. Armand, Z. Zhou, Single lithium-ion conducting solid polymer electrolytes: advances and perspectives, *Chem. Soc. Rev.* 46 (2017) 797–815.
- [17] E. Simonetti, M. Carewska, M. Di Carli, M. Moreno, M. De Francesco, G.B. Appetecchi, Towards improvement of the electrochemical properties of ionic liquid-containing polyethylene oxide-based electrolytes, *Electrochim. Acta* 235 (2017) 323–331.
- [18] Q. Lu, Y.B. He, Q. Yu, B. Li, Y.V. Kaneti, Y. Yao, F. Kang, Q.H. Yang, Dendrite-free, high-rate, long-life lithium metal batteries with a 3D cross-linked network polymer electrolyte, *Adv. Mater.* 29 (2017).

- [19] P.-Y. Ji, J. Fang, Y.-Y. Zhang, P. Zhang, J. Zhao, Novel single lithium-ion conducting polymer electrolyte based on poly(hexafluorobutyl methacrylate-co-lithium allyl sulfonate) for lithium-ion batteries, *ChemElectroChem* (2017).
- [20] J.L. Hu, J. Tian, C.L. Li, Nanostructured carbon nitride polymer-reinforced electrolyte to enable dendrite-suppressed lithium metal batteries, *ACS Appl. Mater. Interfaces* 9 (2017) 11615–11625.
- [21] R. Rohan, K. Pareek, Z.X. Chen, W.W. Cai, Y.F. Zhang, G.D. Xu, Z.Q. Gao, H.S. Cheng, A high performance polysiloxane-based single ion conducting polymeric electrolyte membrane for application in lithium ion batteries, *J. Mater. Chem. A* 3 (2015) 20267–20276.
- [22] Y. Zhang, R. Rohan, W. Cai, G. Xu, Y. Sun, A. Lin, H. Cheng, Influence of chemical microstructure of single-ion polymeric electrolyte membranes on performance of lithium-ion batteries, *ACS Appl. Mater. Interfaces* 6 (2014) 17534–17542.
- [23] R. Rohan, Y.B. Sun, W.W. Cai, K. Pareek, Y.F. Zhang, G.D. Xu, H.S. Cheng, Functionalized meso/macro-porous single ion polymeric electrolyte for applications in lithium ion batteries, *J. Mater. Chem. A* 2 (2014) 2960–2967.
- [24] X.J. Ma, P. Kolla, R.D. Yang, Z. Wang, Y. Zhao, A.L. Smirnova, H. Fong, Electrospun polyacrylonitrile nanofibrous membranes with varied fiber diameters and different membrane porosities as lithium-ion battery separators, *Electrochim. Acta* 236 (2017) 417–423.
- [25] K. Liu, W. Liu, Y. Qiu, B. Kong, Y. Sun, Z. Chen, D. Zhuo, D. Lin, Y. Cui, Electrospun core-shell microfiber separator with thermal-triggered flame-retardant properties for lithium-ion batteries, *Sci. Adv.* 3 (2017).
- [26] D. Wu, C. Shi, S. Huang, X. Qiu, H. Wang, Z. Zhan, P. Zhang, J. Zhao, D. Sun, L. Lin, Electrospun nanofibers for sandwiched polyimide/poly(vinylidene fluoride)/polyimide separators with the thermal shutdown function, *Electrochim. Acta* 176 (2015) 727–734.
- [27] C. Shi, P. Zhang, S. Huang, X. He, P. Yang, D. Wu, D. Sun, J. Zhao, Functional separator consisted of polyimide nonwoven fabrics and polyethylene coating layer for lithium-ion batteries, *J. Power Sources* 298 (2015) 158–165.
- [28] S.W. Choi, S.M. Jo, W.S. Lee, Y.-R. Kim, An electrospun poly(vinylidene fluoride) nanofibrous membrane and its battery applications, *Adv. Mater. (Weinheim, Ger.)* 15 (2003) 2027–2032.
- [29] N. Wu, Q. Cao, X.Y. Wang, X.Y. Li, H.Y. Deng, A novel high-performance gel polymer electrolyte membrane basing on electrospinning technique for lithium rechargeable batteries, *J. Power Sources* 196 (2011) 8638–8643.
- [30] C. Shi, P. Zhang, L. Chen, P. Yang, J. Zhao, Effect of a thin ceramic-coating layer on thermal and electrochemical properties of polyethylene separator for lithium-ion batteries, *J. Power Sources* 270 (2014) 547–553.
- [31] J. Dai, C. Shi, C. Li, X. Shen, L. Peng, D. Wu, D. Sun, P. Zhang, J. Zhao, A rational design of separator with substantially enhanced thermal features for lithium-ion batteries by the polydopamine-ceramic composite modification of polyolefin membranes, *Energy Environ. Sci.* 9 (2016) 3252–3261.
- [32] X. Li, J. He, D. Wu, M. Zhang, J. Meng, P. Ni, Development of plasma-treated polypropylene nonwoven-based composites for high-performance lithium-ion battery separators, *Electrochim. Acta* 167 (2015) 396–403.
- [33] L. Wen, M. Zhou, C. Wang, Y. Mi, Y. Lei, nanoengineering energy conversion and storage devices via atomic layer deposition, *Adv. Energy Mater.* (2016).
- [34] X. Wang, G. Yushin, Chemical vapor deposition and atomic layer deposition for advanced lithium ion batteries and supercapacitors, *Energy Environ. Sci.* 8 (2015) 1889–1904.
- [35] T. Kobayashi, T. Kumazawa, Z.J.L. Kao, T. Nakada, Cu (In, Ga) Se₂ thin film solar cells with a combined ALD-Zn (O, S) buffer and MOCVD-ZnO: B window layers, *Sol. Energy Mat. Sol. C* 119 (2013) 129–133.
- [36] M.E. Donders, W.M. Arnoldbik, H.C.M. Knoops, W.M.M. Kessels, P.H.L. Nottenb, Atomic layer deposition of LiCoO₂ thin-film electrodes for all-solid-state Li-ion micro-batteries, *J. Electrochem. Soc.* 160 (2013) A3066–A3071.
- [37] Y.T. Su, S.H. Cui, Z.Q. Zhuo, W.L. Yang, X.W. Wang, F. Pan, Enhancing the high-voltage cycling performance of LiNi_{0.5}Mn_{0.3}Co_{0.2}O₂ by retarding its interfacial reaction with an electrolyte by atomic-layer-deposited Al₂O₃, *ACS Appl. Mater. Interfaces* 7 (2015) 25105–25112.
- [38] H.Y. Wang, F.M. Wang, Electrochemical investigation of an artificial solid electrolyte interface for improving the cycle-ability of lithium ion batteries using an atomic layer deposition on a graphite electrode, *J. Power Sources* 233 (2013) 1–5.
- [39] D.K. Nandi, U.K. Sen, D. Choudhury, S. Mitra, S.K. Sarkar, Atomic layer deposited molybdenum nitride thin film: a promising anode material for Li ion batteries, *ACS Appl. Mater. Interfaces* 6 (2014) 6606–6615.
- [40] Y.S. Jung, A.S. Cavanagh, L. Gedvilas, N.E. Widjonarko, I.D. Scott, S.H. Lee, G.H. Kim, S.M. George, A.C. Dillon, Improved functionality of lithium-ion batteries enabled by atomic layer deposition on the porous microstructure of polymer separators and coating electrodes, *Adv. Energy Mater.* 2 (2012) 1022–1027.
- [41] H. Chen, L. Kong, Y. Wang, Enhancing the hydrophilicity and water permeability of polypropylene membranes by nitric acid activation and metal oxide deposition, *J. Membr. Sci.* 487 (2015) 109–116.
- [42] H. Chen, Q. Lin, Q. Xu, Y. Yang, Z. Shao, Y. Wang, Plasma activation and atomic layer deposition of TiO₂ on polypropylene membranes for improved performances of lithium-ion batteries, *J. Membr. Sci.* 458 (2014) 217–224.
- [43] X. Meng, X.Q. Yang, X. Sun, Emerging applications of atomic layer deposition for lithium-ion battery studies, *Adv. Mater.* 24 (2012) 3589–3615.
- [44] X. Meng, X. Wang, D. Geng, C. Ozgit-Akgun, N. Schneider, J.W. Elam, Atomic layer deposition for nanomaterial synthesis and functionalization in energy technology, *Mater. Horizons* 4 (2017) 133–154.
- [45] V. Aravindan, K.B. Jinesh, R.R. Prabhakar, V.S. Kale, S. Madhavi, Atomic layer deposited (ALD) SnO₂ anodes with exceptional cycleability for Li-ion batteries, *Nano Energy* 2 (2013) 720–725.
- [46] D.M. Correia, C. Ribeiro, V. Sencadas, G. Botelho, S.A.C. Carabineiro, J.L.G. Ribelles, S. Lanceros-Méndez, Influence of oxygen plasma treatment parameters on poly(vinylidene fluoride) electrospun fiber mats wettability, *Prog. Org. Coat.* 85 (2015) 151–158.
- [47] Y.W. Park, N. Inagaki, Surface modification of poly(vinylidene fluoride) film by remote Ar, H-2, and O-2 plasmas, *Polymer* 44 (2003) 1569–1575.